Molecular beam epitaxy of ferromagnetic γ'-Fe_4N thin films on $LaAlO_3$(100), $SrTiO_3$(100) and MgO(100) substrates

Keita Ito[a], Geun Hyoung Lee[a], Hiro Akinaga[b], Takashi Suemasu[a]

[a]*Institute of Applied Physics, University of Tsukuba, 1-1-1 Tennohdai, Tsukuba, Ibaraki 305-8573, Japan*

[b]*National Institute of Advanced Industrial Science and Technology (AIST), NIRC, 1-1-1 Umezono, Tsukuba, Ibaraki 305-8568, Japan*

Keywords: MBE, γ'-Fe_4N, $LaAlO_3$, $SrTiO_3$, MgO, spintronics

We have attempted to grow *a*-axis-oriented γ'-Fe_4N epitaxial films with smooth surfaces at around 400 °C on $LaAlO_3$ (LAO)(100), $SrTiO_3$ (STO)(100) and MgO(100) substrates by molecular beam epitaxy using solid Fe and a radio-frequency NH_3 plasma as the Fe and N sources, respectively. The lattice mismatch of these substrates to γ'-Fe_4N is 0, 3 and 11%, respectively. Epitaxial growth of γ'-Fe_4N films was successfully achieved on the STO(100) and LAO(100) substrates. It was found from reflection high-energy electron diffraction and x-ray diffraction that the *a*-axis orientation of γ'-Fe_4N was degraded with increasing lattice mismatch. High-angle annular dark-field scanning transmission electron microscopy and

electron energy-loss spectroscopy measurements showed that amorphous Al-O layers were present at the γ'-Fe_4N/LAO interface.

1. Introduction

In recent years, spintronics, which is an emerging area of electronics with the potential for new functional devices such as spin random access memory (Spin-RAM) and spin transistors by the creation and control of electron spin, has attracted significant attention. The use of ferromagnetic materials with high spin polarization and low lattice mismatch to Si as effective spin injection electrodes for Si is appropriate. In particular, special attention has been paid to ferromagnetic γ'-Fe_4N as a spin injection electrode for Si. γ'-Fe_4N is chemically stable and has a relatively small lattice mismatch of 1.3% to Si(100), and the Curie temperature is reported to be 767 K [1]. Very recently, we have confirmed, from point-contact Andreev reflection measurements, that spin polarization in highly *a*-axis-oriented polycrystalline γ'-Fe_4N thin films grown by molecular beam epitaxy (MBE) is larger than that in α-Fe [2]. According to Kokado *et al.*, the electrical conductivities of *up* spins and *down* spins in γ'-Fe_4N were theoretically calculated, and spin polarization of the electrical conductivity at the Fermi level is −1.0 [3]. Furthermore, an inverse tunneling magnetoresistance ratio of −75% due to negative spin polarization of γ'-Fe_4N was reported at RT in CoFeB/MgO/γ'-Fe_4N magnetic tunnel junctions fabricated by sputtering [4]. Therefore, γ'-Fe_4N is considered to be an appropriate material for application in Si-based spintronics devices [5].

However, the magnetic moments of γ'-Fe_4N remain unclear from an experimental

point of view. Atiq *et al*. fabricated γ'-Fe_4N films on (100) faces of $LaAlO_3$(LAO), $SrTiO_3$ (STO) and MgO substrates by sputtering, and reported that the saturation magnetization per unit volume (M_s) in γ'-Fe_4N increases with decreasing lattice mismatch between γ'-Fe_4N and the substrate used. The lattice mismatch was approximately 0, 3 and 11%, respectively, for the three substrates [6]. We believe high-quality γ'-Fe_4N epitaxial films should be employed to confirm this experimental result, and also to investigate their applicability as spin injection electrodes. There have been many reports on the growth of γ'-Fe_4N thin films on MgO(100) [6-8], STO (100) [6,9], LAO (100) [6], Cu(100) [10] and Si(100) [11] substrates by MBE, sputtering, chemical vapor deposition etc. However, there are few papers on epitaxial growth of γ'-Fe_4N thin films [6-10]. There are no reports so far on the epitaxial growth of γ'-Fe_4N thin films on LAO and STO by MBE. The purpose of this work is to achieve epitaxial growth of γ'-Fe_4N thin films on LAO(100), STO(100) and MgO(100) substrates by MBE. Very thin films of LAO and STO can be utilized as a tunnel barrier layer between γ'-Fe_4N and Si(100) due to their small lattice mismatch to both γ'-Fe_4N and Si(100).

2. Experimental procedures

An ion-pumped MBE system equipped with a high-temperature Knudsen cell for 5N-Fe and a radio-frequency (RF) NH_3 plasma for N was used. Thin films of γ'-Fe_4N (samples A–I) were grown on LAO(100), STO(100) and MgO(100) substrates by supplying

Fe and N simultaneously in a stoichiometric proportion. Prior to the fabrication of the γ'-Fe_4N layers, the three substrates were processed differently. STO(100) substrates were dipped into a buffered HF (HF = 5 wt%, NH_4F = 35 wt%) solution and heated at 900 °C for 30 min under an oxygen partial pressure of 5×10^{-6} Torr, in order to get an atomically flat surface [12,13]. MgO(001) substrates were heated at 900 °C for 30 min in an ultrahigh vacuum. In contrast, for LAO(100) substrates, such a high temperature pre-annealing was not performed, in order to prevent crack formation. The substrate temperature during the growth was optimized in order to get good crystallization and flat surfaces. After several trials, we determined that 375, 400 and 415 °C were suitable temperature for γ'-Fe_4N layer growth on LAO (samples A and G), STO (samples B and H) and MgO (samples C and I), respectively. Table 1 summarizes the growth conditions used for the samples and substrates. The crystalline quality of the γ'-Fe_4N was evaluated from reflection high-energy electron diffraction (RHEED) measurements, x-ray diffraction (XRD) measurements, and atomic force microscopy (AFM). For samples G–I, the γ'-Fe_4N films were capped with a 3-nm-thick Au layer to prevent oxidation on the surface, and cross-sectional transmission electron microscopy (TEM), high-angle annular dark-field scanning transmission electron microscopy (HAADF-STEM) and electron energy-loss spectroscopy (EELS) measurements were carried out.

3. Results and discussion

Fig. 1(a-c) show typical examples of RHEED patterns observed for samples A-C. Streaky patterns were observed for samples A and B with γ'-Fe_4N layers grown on LAO(100) and STO(100) substrates, respectively. On the other hand, γ'-Fe_4N layers on MgO(100), sample C, showed a spotty pattern together with a ring structure, meaning that the γ'-Fe_4N rotates along the surface normal. The θ-2θ XRD patterns from samples A-C are shown in Fig. 2(a-c). No diffraction peaks corresponding to α-Fe and iron nitrides, other than γ'-Fe_4N, were observed in the samples. Due to the very close lattice constant values between LAO and γ'-Fe_4N as well as the *a*-axis orientation of γ'-Fe_4N, the diffraction peaks due to γ'-Fe_4N overlap the (100)-oriented diffraction peaks of the LAO substrate. Intense diffraction peaks of (100)-oriented γ'-Fe_4N such as (200) and (400) are clearly seen for sample B with the STO(100) substrate. In contrast to γ'-Fe_4N/STO(100), the peak intensity of γ'-Fe_4N(200) for sample C, grown on the MgO(001) substrate, is significantly smaller.

The surfaces of samples A-C were relatively smooth. Fig. 3(a–c) show AFM images of samples A–C. The root-mean-square (RMS) values of the surface roughness were found to be approximately 0.25 nm for each sample. Step and terrace structures were observed for the γ'-Fe_4N surface in sample A with the LAO(100) substrate, as seen in Fig. 3(a). On the basis of these results, we conclude that epitaxial (100)-oriented γ'-Fe_4N films with smooth surfaces were successfully grown on LAO(100) and STO(100) substrates.

We next consider the influence of lattice mismatch on the *a*-axis orientation of

γ'-Fe_4N and the strain within the γ'-Fe_4N layers. Fig. 4(a-c) show x-ray rocking curves for the γ'-Fe_4N(200) plane in samples D-F. Ge(220) single crystals were used to make the incident x-rays parallel in the XRD equipment. The full width at half maximum (FWHM) for 14-nm-thick γ'-Fe_4N layers, sample D, grown on an MgO(100) substrate was more than 10°. This implies that the *a*-axis of the γ'-Fe_4N layers on MgO(100) tilted significantly with respect to the surface normal. In contrast, the FWHM for 12-nm-thick γ'-Fe_4N layers on STO(100), sample E, was approximately 2°, and the FWHM value decreased further to 0.99° with increasing γ'-Fe_4N layer thickness to 30 nm in sample F. These results show that the *a*-axis orientation of γ'-Fe_4N degraded with increasing lattice mismatch between γ'-Fe_4N and the substrate used. Fig. 5(a) and (b) show x-ray reciprocal lattice mappings for a 12-nm-thick γ'-Fe_4N layer, sample E, and a 30-nm-thick γ'-Fe_4N layer, sample F, on STO(100). Considering that the γ'-Fe_4N layers are epitaxially grown on STO(100) with the *a*-axis normal to the sample surface, the γ'-Fe_4N (113) and STO(113) spots should be on the same vertical line if the lattice constants *b* and *c* of γ'-Fe_4N in the lateral direction are equal to those of STO(100). However, as seen in Fig. 5(a) and (b), the γ'-Fe_4N (113) and STO(113) spots are not on the vertical broken line, but rather on the inclined broken line which crosses the origin of the reciprocal lattice. This indicates that the γ'-Fe_4N layers in samples E and F are not strained but are fully relaxed.

Fig. 6(a-c) show cross-sectional TEM images of samples G-I. The γ'-Fe_4N layers in

these samples were covered with 3-nm-thick Au capping layers. As shown in Fig. 6(a), we can clearly see a very thin interfacial layer between the γ'-Fe_4N layers and the LAO(100) substrate in sample G. Fig. 7(a) and (b) show HAADF-STEM images of sample G at low magnification and at high magnification, respectively. In HAADF-STEM images, it is well known that heavy atoms such as La and Fe appear brighter. In the present work, we can see clear lattice images inside the γ'-Fe_4N layers and the LAO substrate, but not around the interface, as shown in Fig. 7(b). Furthermore, around the interface the image is darker than the other areas, indicating that the interfacial layers are amorphous and probably consist of light atoms such as Al. Fig. 7(c) shows EELS depth profiles of Fe, N, La and O atoms observed for sample G. An EELS line scan was performed along the white line shown in Fig. 7(a). From comparison of the profile of O atoms with that of La atoms, it was found that O atoms diffused slightly into the γ'-Fe_4N layers from the LAO substrate. From the HAADF-STEM and EELS analyses results for sample G, we can say that amorphous Al-O layers are likely present at the γ'-Fe_4N/LAO(100) interface. We should also note that the Fe atoms were not uniform in the γ'-Fe_4N layers near the interface. We believe that the diffusion of O atoms into the γ'-Fe_4N layers may affect the profile of the Fe atoms. On the basis of all experimental results in this work, we conclude that γ'-Fe_4N thin films grown on a STO(100) substrate have better crystalline quality than those grown on LAO(100) and MgO(100) substrates.

4. Conclusions

We have succeeded in growing *a*-axis-oriented γ'-Fe_4N films epitaxially on LAO(100) and STO(100) substrates by MBE using 5N-Fe and RF-NH_3 as Fe and N sources respectively. In contrast, RHEED and XRD patterns revealed that it was difficult to grow γ'-Fe_4N films epitaxially on MgO(100) substrates. These results imply that the *a*-axis orientation of γ'-Fe_4N was degraded with increasing lattice mismatch. From reciprocal lattice mappings for 14-nm-thick and 30-nm-thick γ'-Fe_4N thin films grown on STO(001) substrates, the γ'-Fe_4N films were found not to be strained. HAADF-STEM and EELS spectroscopy measurements indicated that amorphous Al-O layers were present at the γ'-Fe_4N/LAO interface.

Acknowledgements

This work was supported in part by a Grant-in-Aid for Scientific Research on the Priority Area of "Creation and Control of Spin Current" (19048029) from the Ministry of Education, Culture, Sports, Science and Technology of Japan (MEXT) and by the NanoProcessing Partnership Platform (NPPP) at AIST, Tsukuba. High-purity 5N Fe was supplied by Prof. M. Isshiki and Dr. M. Uchikoshi of Tohoku University. Several XRD measurements were done with the help of the Rigaku Corporation. The authors also thank Dr.

N. Ota and Prof. K. Asakawa of the Tsukuba Nano-Tech Human Resource Development Program at the University of Tsukuba for useful discussions.

References

[1] G. Shirane, W. J. Takei, S. L. Ruby, Phys. Rev. 126 (1962) 49.

[2] A. Narahara, K. Ito, T. Suemasu, Y. K. Takahashi, A. Rajanikanth, K. Hono, Appl. Phys. Lett. 94 (2009) 202502.

[3] S. Kokado, N. Fujima, K. Harigaya, H. Shimizu, A. Sakuma, Phys. Rev. B 73 (2006) 172410.

[4] Y. Komasaki, M. Tsunoda, S. Isogami, M. Takahashi, J. Appl. Phys. 105 (2009) 07C928.

[5] *INTERNATIONAL TECHNOLOGY ROADMAP FOR SEMICONDUCTORS, 2009 EDITION p. 13*.

[6] S. Atiq, H. S. Ko, S. A. Siddiqi, S. C. Shin, Appl. Phys. Lett. 92 (2008) 222507.

[7] D. M. Borsa, S. Grachev, D. O. Boerma, J. W. J. Kerssemakers, Appl. Phys. Lett. 79 (2001) 994.

[8] T. Takahashi, N. Takahashi, N. Tamura, T. Nakamura, M. Yoshioka, W. Inami, Y. Kawata, J. Mater. Chemistry 11 (2001) 3154.

[9] K. R. Nikolaev, I. N. Krivorotov, E. D. Dahlberg, V. A. Vas'ko, S. Urazhdin, R. Loloee, W. P. Pratt Jr., Appl. Phys. Lett. 82 (2003) 4534.

[10] J. M Gallego, S. Y. Grachev, D. M. Borsa, D. O. Boerma, D. E´cija, R. Miranda, Phys. Rev. B 70 (2004) 115417.

[11] L. L. Wang, W. T. Zheng, J. Gong, H .B. Li, X. Wang, N. Ma, P. J. Cao, X. C. Ma, J.

Alloys. Compd. 467 (2009) 1.

[12] M. Kawasaki, K. Takahashi, T. Maeda, R. Tsuchiya, M. Shinohara, O. Ishiyama, T. Yonezawa, M. Yoshimoto, H. Koinuma, Science 266 (1994) 1540.

[13] S. Y. Jang, N. Nakagawa, S. J. Moon, T. Susaki, K. W. Kim, Y. S. Lee, H. Y. Hwang, K. M. Whun, Solid State Commun. 149 (2009) 1760.

Fig. 1. RHEED patterns from samples (a) A, (b) B and (c) C taken from the [100] azimuth of γ'-Fe_4N.

Fig. 2. θ-2θ XRD patterns for samples (a) A, (b) B and (c) C.

Fig. 3. AFM images of samples (a) A, (b) B and (c) C. RMS values of surface roughness were 0.24, 0.26 and 0.26 nm, respectively.

Fig. 4. X-ray rocking curves for samples (a) D, (b) E and (c) F for γ'-Fe_4N(200).

Fig. 5. X-ray reciprocal lattice mappings for samples (a) E and (b) F.

Fig. 6. Cross-sectional TEM images of samples (a) G, (b) H and (c) I. The electron beam was incident along the [100] azimuth of γ'-Fe_4N.

Fig. 7. Cross-sectional HAADF-STEM images of sample G at (a) low magnification and (b) high magnification. The electron beam was incident along the γ'-Fe_4N [100] azimuth. Heavy atoms appear brighter than light atoms. (c) EELS depth profiles of Fe, N, La and O atoms observed for sample G along the white line.

Table 1 Growth conditions used for the samples. Samples A and G were grown on LAO substrates. Samples B, E, F and H were grown on STO substrates. Samples C and I were grown on MgO substrates. In samples G-I, γ'-Fe_4N layers were covered with Au capping layers.

Sample	Substrate	Growth temperature(°C)	γ'-Fe_4N layer (nm)	Au layer (nm)
Sample A	LAO(100)	375	8	-
Sample B	STO(100)	400	12	-
Sample C	MgO(100)	415	10	-
Sample D	MgO(100)	450	14	-
Sample E	STO(100)	450	12	-
Sample F	STO(100)	450	30	-
Sample G	LAO(100)	375	11	3
Sample H	STO(100)	400	11	3
Sample I	MgO(100)	415	10	3

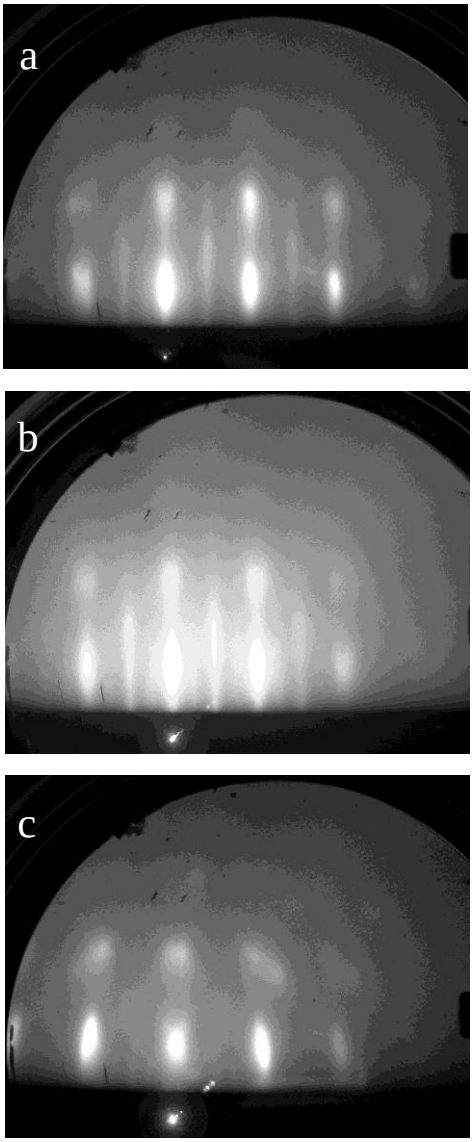

Fig. 1

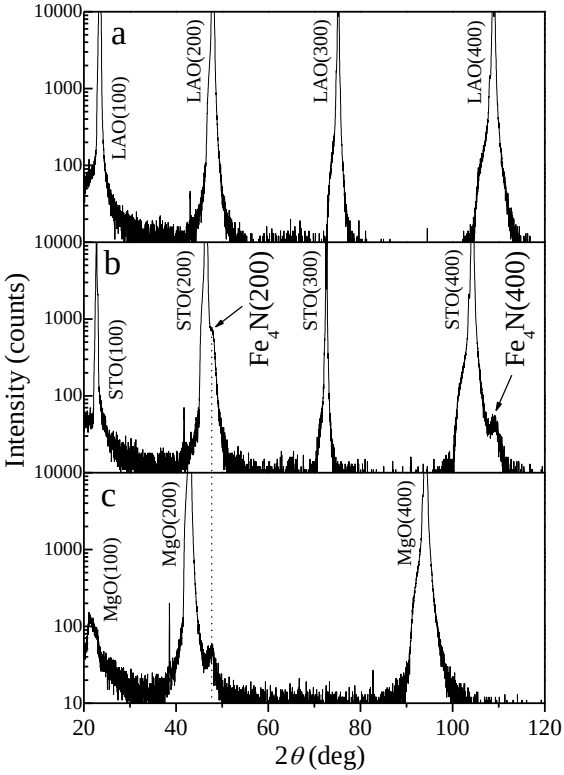
a
b
c
LAO(100)
LAO(200)
LAO(300)
LAO(400)
STO(100)
STO(200)
STO(300)
STO(400)
Fe4N(200)
Fe4N(400)
MgO(100)
MgO(200)
MgO(400)
Intensity (counts)
2θ (deg)
10000
1000
100
10
20
40
60
80
100
120

Fig. 2

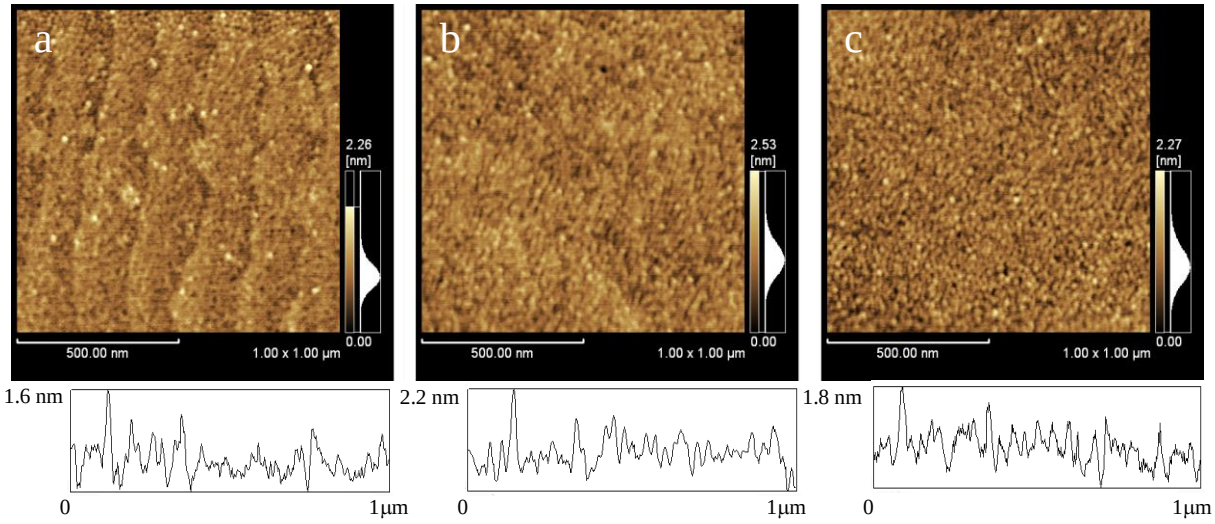
a
2.26
[nm]
0.00
500.00 nm
1.00 x 1.00 µm
b
2.53
[nm]
0.00
500.00 nm
1.00 x 1.00 µm
c
2.27
[nm]
0.00
500.00 nm
1.00 x 1.00 µm
1.6 nm
0
1µm
2.2 nm
0
1µm
1.8 nm
0
1µm

Fig.3

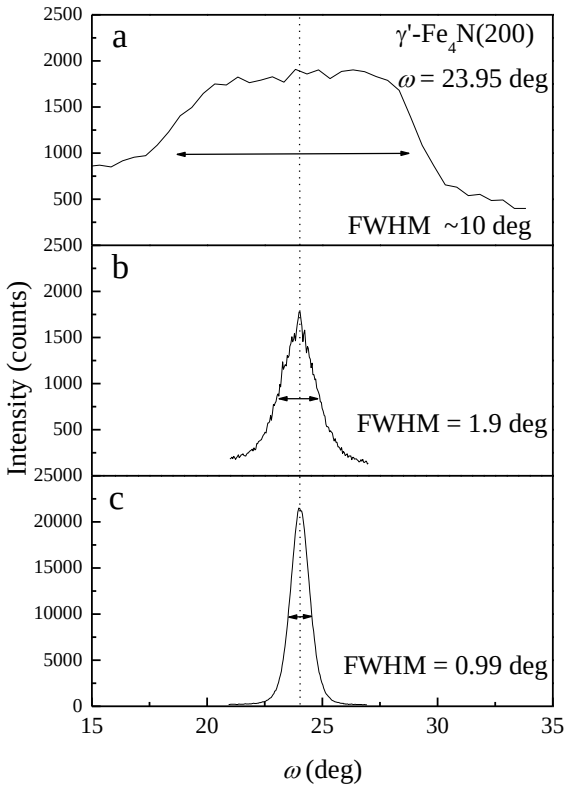
a
γ'-Fe4N(200)
ω = 23.95 deg
FWHM ~10 deg
b
FWHM = 1.9 deg
c
FWHM = 0.99 deg
Intensity (counts)
ω (deg)
2500
2000
1500
1000
500
25000
20000
15000
10000
5000
0
15
20
25
30
35

Fig. 4

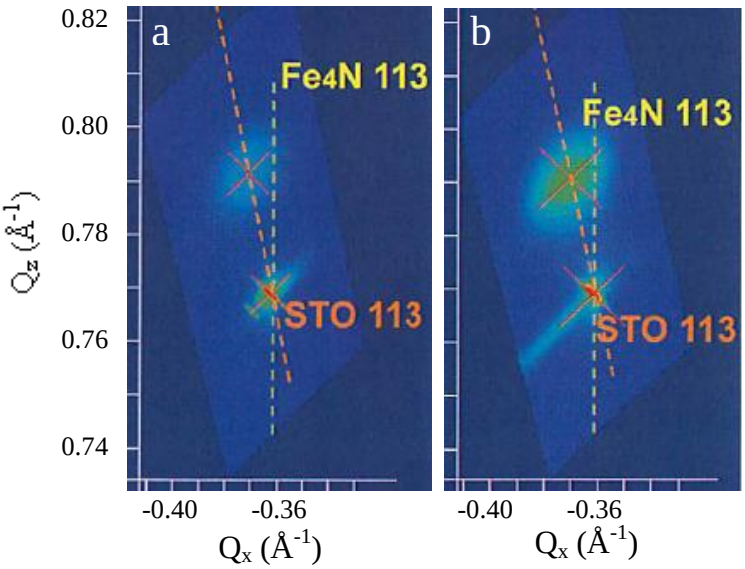
a
b
Fe4N 113
Fe4N 113
STO 113
STO 113
0.82
0.80
0.78
0.76
0.74
Qz (Å-1)
-0.40
-0.36
-0.40
-0.36
Qx (Å-1)
Qx (Å-1)

Fig. 5.

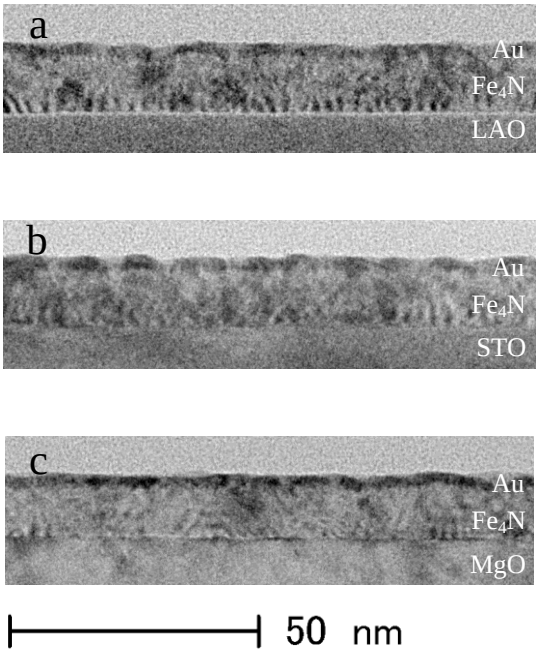

Fig. 6

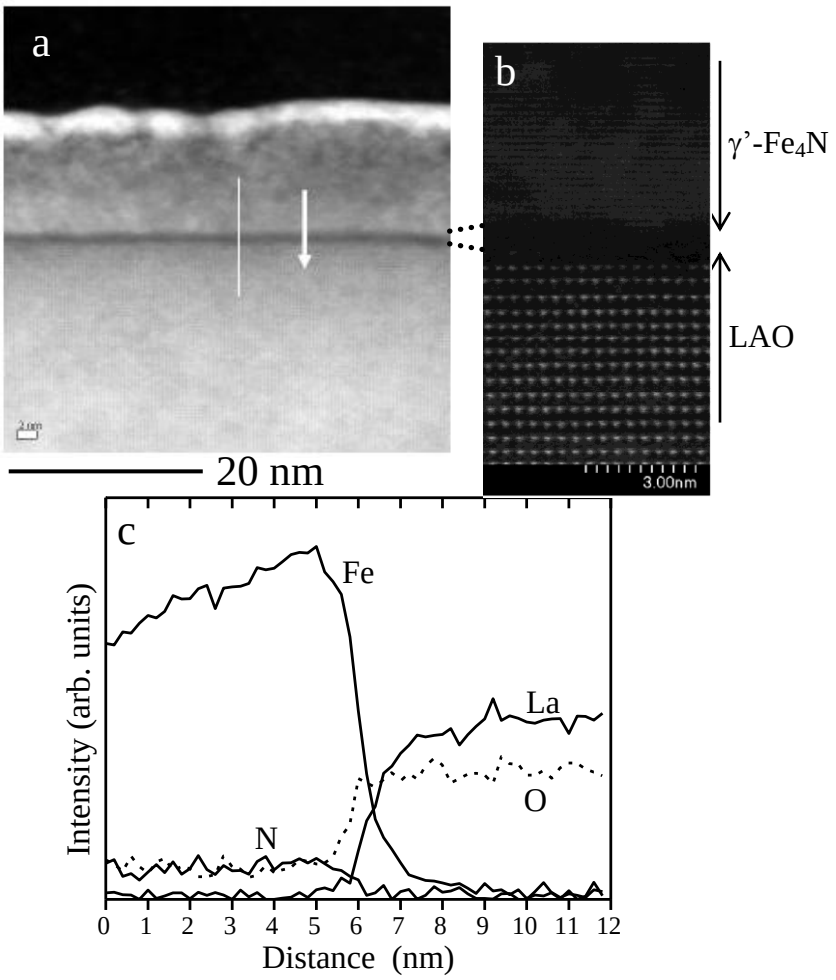
a
b
γ'-Fe4N
LAO
3.00nm
20 nm
c
Fe
La
O
N
Intensity (arb. units)
0 1 2 3 4 5 6 7 8 9 10 11 12
Distance (nm)

Fig. 7